BULLETIN OF THE POLISH ACADEMY OF SCIENCES
TECHNICAL SCIENCES, Vol. 68, No. 3, 2020
DOI: 10.24425/bpasts.2020.133367

Fractional discrete model of an electrical drive with brushless micro-motor

M. MATUSIAK*, M. BĄKAŁA, R. WOJCIECHOWSKI, and P. OSTALCZYK

Institute of Applied Computer Science, Lodz University of Technology, ul. Stefanowskiego 18/22, 90-924 Łódź, Poland

Abstract. The use of fractional-order calculus for system modeling is a good alternative to well-known classic integer-order methods, primarily due to the precision with which the modeled object may be mapped. In this study, we created integer and fractional discrete models of a real object – a highspeed brushless micro-motor. The accuracy of the models was verified and compared.

Key words: system modeling, system identification, fractional order calculus.

1. Introduction

The application of fractional-order calculus (FOC) in control theory and engineering has been the subject of growing interest in recent years, due to its proven advantages over classical integer-order calculus, especially as a mathematical tool for the synthesis of dynamical models and the design of sophisticated control laws [1–5]. A number of studies have proven the robustness, performance, and accuracy of such models and controllers, most recently [6–11]. Despite the obvious advantages of FOC-based models, a major challenge is still the complexity of calculating fractional differintegral equations. Common approaches to solving this problem include applying short memory methods to simplify the calculations or using integer-order approximations for fractional operator s^{ν}. The digital implementation of FOC equations, not only in theory, but in real devices, has been dealt with in only a small number of works [10, 12–18].

In this study, a sophisticated laboratory stand for research on FOC applications was designed, with a fast brushless direct-current (BLDC) micromotor as the target modeled system. Based on real system responses, well-known classical integer models – first order plus dead time (FOPDT), second order plus dead time (SOPDT) – as well as fractional-order models were constructed. Identification of the plant was performed using classic integer-order Küpfmüller models and verified with the prediction error method (PEM) algorithm in the PID Tuner applet of the MATLAB System Identification Toolbox [19]. Synthesis of the final fractional-order form of the model was achieved by minimizing the chosen error cost function, evaluated using the Grünwald-Letnikov algorithm in the FOMCON toolbox [20–22]. All the models were verified for accuracy against measurements of real objects.

In Section 2 of the paper, the mathematical preliminaries related to fractional calculus and fractional-order systems are laid out. Next, a physical model of the laboratory stand is described in detail. Usage of different types of the model for plant identification are discussed in Section 4. All proposed models have been verified for accuracy and presented as indicators and performance indices, in terms of max absolute percentages and square root means. The final section draws conclusions from the results.

2. Mathematical preliminaries

Three definitions of fractional differintegral operators are widely known and applied: Grünwald–Letnikov (GL), Riemann–Liouville (RL) and Caputo (C). We will focus on the first definition, a generalization of the classic derivative of the n-th $(n \in \mathbb{N})$ order to a derivative of an arbitrary real order $\nu \in \mathbb{R}_+$. This form is most convenient for digital implementation [1–3, 23].

Definition 1. Grünwald–Letnikov classic fractional differintegral operator

$$
\begin{aligned}
{}^{GL}D^{\nu} f(t) &= \lim_{h\to 0} \frac{1}{h^{\nu}} \sum_{j=0}^{\infty} (-1)^j \binom{\nu}{j} f\big((k-j)h\big) = \\
&= \lim_{h\to 0} \frac{1}{h^{\nu}} \sum_{j=0}^{\infty} (-1)^j \frac{\nu(\nu-1)\ldots(\nu-j+1)}{j!} f\big((k-j)h\big) = \\
&= \lim_{h\to 0} \frac{1}{h^{\nu}} \sum_{j=0}^{\infty} (-1)^j \frac{\Gamma(\nu+1)}{j!\,\Gamma(\nu-j+1)} f\big((k-j)h\big) = \\
&= \sum_{j=0}^{\infty} a_j f\big((k-j)h\big) \qquad (1)
\end{aligned}
$$

where: $t = kh$, $h \in \mathbb{R}_+$ denotes the sampling period, which is constant, finite, and as small as possible, and $a_j = (-1)^j \binom{\nu}{j}$.

*e-mail: mmatusiak@iis.p.lodz.pl

Manuscript submitted 2020-01-14, revised 2020-03-22, initially accepted for publication 2020-04-15, published in June 2020

In practical applications, usually the starting point is $t_0 = 0$ and the values of the function $f(t)$ are not defined in the range $t \in (-\infty, t_0)$. Therefore, a truncated form of Definition 1 is of great interest.

Definition 2. Grünwald–Letnikov truncated fractional differintegral operator

$$ {}^{GL}_{t_0}D^{\nu}_t f(t) = \lim_{h\to 0} \frac{1}{h^{\nu}} \sum_{j=0}^{N} (-1)^j f\big((k-j)h\big) \tag{2} $$

where $N = \left[\dfrac{t-t_0}{h}\right]$.

To avoid problems relating to the finite range and precision of numbers in computing, the factorial value in (1) and (2) on a microcontroller, a slightly modified form shall be considered, which uses recursively computed weights [2, 24–26]:

$$ {}^{GL}_{t_0}D^{\nu}_t f(t) \approx \frac{1}{h^{\nu}} \sum_{j=0}^{N} a^{\nu}_j f\big((k-j)h\big), \tag{3} $$

$$ a^{\nu}_j = \begin{cases} 1, & \text{for } j = 0 \\ a^{\nu}_{j-1}\left(1 - \dfrac{1+\nu}{j}\right), & \text{for } j = 1,2,\ldots \end{cases} $$

(1)–(3) can be also expressed in matrix algebra form:

$$ {}^{GL}_{t_0}D^{\nu}_t f(t) = \frac{1}{h^{\nu}} \begin{bmatrix} a^{\nu}_0 & a^{\nu}_1 & \ldots & a^{\nu}_N \end{bmatrix} \begin{bmatrix} f(t) \\ f(t-h) \\ \vdots \\ f(0) \end{bmatrix}. \tag{4} $$

In [27, 28], it was shown that by evaluating fractional-order derivatives of several proposed elementary functions using simplified (finite memory) forms of GL and Horner definitions one can obtain a better approximation accuracy with fewer coefficients and samples processed using the later algorithm. The Grünwald-Letnikov formula (3) requires computing discrete convolution of function $f(kh)$ using a set of coefficients with lengths over 600 to provide satisfactory results. In general, the accuracy depends closely on several factors, the most important of which are the selected value for the fractional order ν [29], the dynamic range of the input signal, and the precision of the numerical calculations.

Let us now consider a dynamical system, described by the fractional-order differential equation:

Definition 3. Fractional-order system, fractional differential equation, and Laplace transform

$$ \begin{aligned} a_n\, {}^{GL}_{t_0}D^{\alpha_n}_t y(t) + a_{n-1}\, {}^{GL}_{t_0}D^{\alpha_{n-1}}_t y(t) + \\ + \ldots + a_0\, {}^{GL}_{t_0}D^{\alpha_0}_t y(t) = b_m\, {}^{GL}_{t_0}D^{\beta_m}_t u(t) + \\ + b_{m-1}\, {}^{GL}_{t_0}D^{\beta_{m-1}}_t u(t) + \ldots + b_0\, {}^{GL}_{t_0}D^{\beta_0}_t u(t). \end{aligned} \tag{5} $$

The system is of a commensurate order if the α_n, β_m orders in the above formula are multiples of a base, real order ν, i.e. $\alpha_k, \beta_k = k\nu$, $\nu \in \mathbb{R}^+$. Moreover, if $\nu = \dfrac{1}{q}$, $q \in \mathbb{Z}^+$ then the system is of the rational order.

Assuming zero initial conditions, the Laplace transform of (1) is defined as:

$$ \mathscr{L}\left\{ {}^{GL}_{t_0}D^{\alpha_n}_t y(t) \right\} = s^{\alpha} F(s). \tag{6} $$

Hence, the fractional-order system can be also described by a continuous transfer function of the form:

$$ \begin{aligned} G(s) &= \frac{b_m s^{\beta_m} + b_{m-1} s^{\beta_{m-1}} + \ldots + b_0 s^{\beta_0}}{a_n s^{\alpha_n} + a_{n-1} s^{\alpha_{n-1}} + \ldots + a_0 s^{\alpha_0}} = \\ &= \frac{\dfrac{b_m}{a_n} s^{\beta_m} + \dfrac{b_{m-1}}{a_n} s^{\beta_{m-1}} + \ldots + \dfrac{b_0}{a_n} s^{\beta_0}}{s^{\alpha_n} + \dfrac{a_{n-1}}{a_n} s^{\alpha_{n-1}} + \ldots + \dfrac{a_0}{a_n} s^{\alpha_0}}. \end{aligned} \tag{7} $$

If the system is of the commensurate-order, then the transfer function $G(s)$ can be rewritten as a pseudo-rational function, $H(\lambda)$, $\lambda = s^{\gamma}$, allowing for example simple migration to a state-space model $H(s) = C(sI - A)^{-1}B + D$.

Theorem 1. Matignon's stability theorem.

Let us consider the fractional-order transfer function of the general form $G(s) = \dfrac{Z(s)}{P(s)}$. The $G(s)$ transfer function is stable if in the σ-plane:

$$ |arg(\sigma)| > q\frac{\pi}{2}, \quad \forall \sigma \in \mathbb{C}, \quad P(\sigma) = 0, \quad \sigma := s^q \tag{8} $$

and $\sigma = 0$ is not a single root of $P(s)$.

3. Physical model of laboratory stand

For the purposes of system modeling using fractional differintegral operators, a laboratory stand was created. In the main part of the stand there are two high-speed brushless DC micromotors, commonly used in the construction of flying objects, installed symmetrically on an adjustable bar (Fig. 1 and Fig. 2).

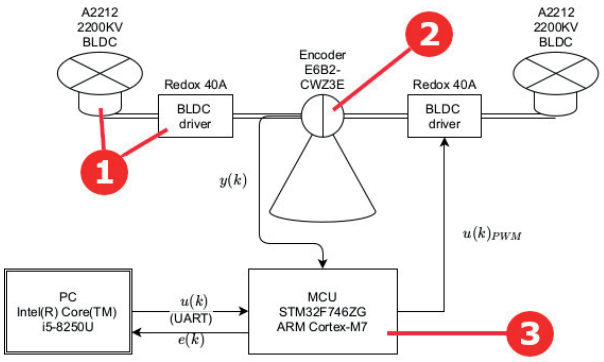

Fig. 1. Block scheme for identification based on the measurement of output samples of plant for a known input signal (1 – BLDC micromotor and driver, 2 – high-precision encoder, 3 – microcontroller)

The first motor acts as the main drive, while the second generates system disturbances in a controlled manner. The bar is connected by the axis of rotation with an incremental encoder, allowing determination of the current angle/position of deflection. The controllers of the encoder and motor are supervised by the STM32F746ZG microcontroller [30]. The basic parameters of the components of the laboratory stand are displayed in Table 1.

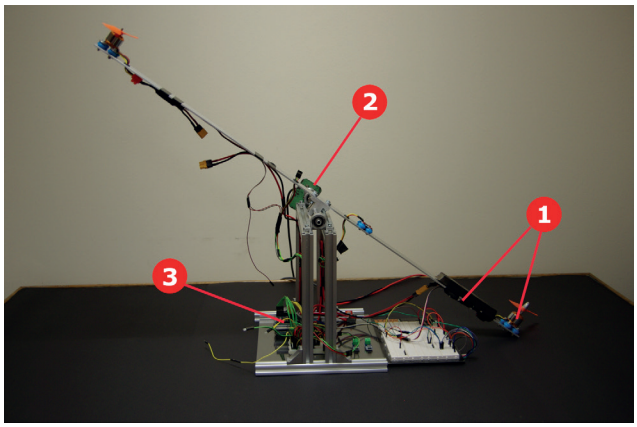

Fig. 2. Overview of the laboratory device (1 – BLDC micromotor and driver, 2 – high-precision encoder, 3 – microcontroller)

Table 1
Selected features of the stand components [30–32]

Microcontroller

Model	STM32F746ZG
CPU	ARM Cortex-M7 32-bit RISC core
CPU frequency	216 MHz
SRAM memory	320KB (including 64KB of data TCM RAM for critical real-time data) 16KB of instruction TCM RAM (for critical real-time routines) 4KB of backup SRAM (available in the lowest power modes)
FLASH memory	1 Mbyte
ADC frequency	108 MHz
ADC sampling time	10 µs
Benchmark	231 DMIPS

Encoder

Model	E6B2-CWZ3E
Type	Incremental
Resolution	1000 P/R

Motor

Model	A2212 2200KV 2-3S
Rotations	2200 RPM/V
Power	220 W
Control	PWM

The physics of the system are described as the resultant of forces acting on its appropriate elements, including the thrust and gravitation related to each motor, and the forces associated with the bar installation including bearing resistance and bar bounce. Due to the system dynamics and lack of detailed specification of its elements, it is impossible to determine an analytical description of the system physics, and for this reason the whole stand is treated as a *black box*, which takes into account the motor settings and responses for the current bar position

4. Plant identification

Identification of the approximated linear model of a BLDC motor treated as a black box (and any other model in general) can be performed in two ways: 1) indirectly, where model of a controller $C(s)$ in a closed-loop system is known and parameters of the plant model $G(s)$ are obtained based on a reference input signal; 2) directly, in an open-loop by measuring output samples of the plant for a known input signal (Fig. 1) [21,33]. Synthesis of the final form of the model is based on finding coefficients of formula (7), so the chosen error cost function (for instance, the least-squares algorithm (LSA)) is minimized:

$$\begin{aligned} e(k) &= y(k) - y_{ref}(k), \\ E_c &\geq LSA = \|e(k)\|_2^2 \end{aligned} \tag{9}$$

where $y(k)$, $y_{ref}(k)$ denote position (angle) of an adjustable bar determined by encoder pulses for a reference signal $u(k)$ and the output of the simulated model, respectively (Fig. 1), and E_c is an arbitrary chosen maximum accepted value of the error norm. Alternatively, the algorithm may be terminated when the desired number of iterations is reached. In this study we followed method 2).

The output data of the described system was the number of encoder impulses, indicating the angular position of the raised arm. The PWM signal connected to the driver of the BLDC had a constant pulse width of 27%. The results of four independent series of measurements are presented in Fig. 3. Series 1–3 indicate repeatability of the measurements, while the series 4 suffered from the external disturbances and was omitted in further analysis.

At time $t_e = 2.6$ s, the PWM control signal was turned off. The data were further processed in MATLAB software. Since the sampling period of the acquisition board was not entirely constant and equaled $t_{s,init} = 10\,\text{ms} \pm \Delta 1\,\text{ms}$, we received a series of non-uniformed data in time. Therefore, the series needed to be resampled, first at a new constant sampling frequency f_s using the linear interpolation method. The value of 1 kHz was chosen and later used also for configuration of the target STM32 microcontroller. In MATLAB, one can obtain interpolated samples by the following procedure:

Listing 1: Signal interpolation (resampling) in Matlab

```
Ts = 0.001;
method = 'linear';
dS = timeseries(msrdData, msrdTime,
```

```
    'Name','Measured data');
newTime = msrdTime(1):Ts:msrdTime(end);
uS = resample(dS, newTime, method);
```

where:

- `Ts` – new sampling period [s],
- `method` – interpolation method (also 'zoh' for zero-order hold),
- `dS` – measured data series,
- `msrdData` – N-element vector of measured samples,
- `msrdTime` – corresponding time vector,
- `newTime` – desired time vector,
- `uS` – new series of unified values.

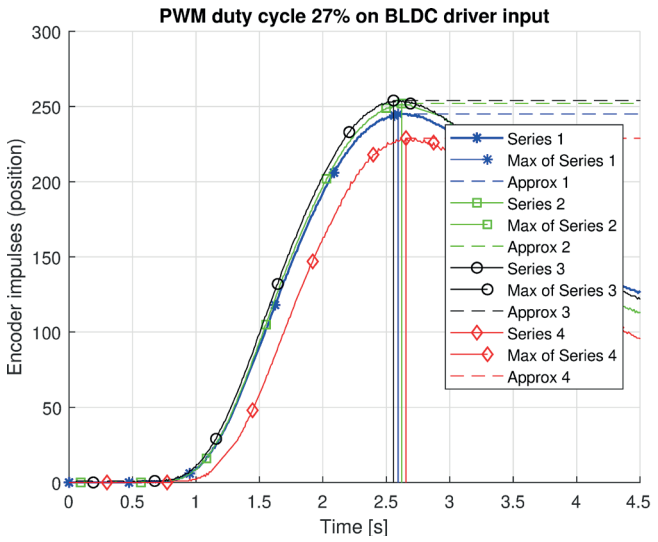

Fig. 3. Measured number of encoder impulses (angle) for the PWM 27% duty cycle

In further experiments, we used Series 1 (see Fig. 3). The `uS` vector was then used to obtain an accurate model of the plant. This procedure resulted in the following formulas:

1. First-order dynamic plant with delay (FOPDT). Identification was performed using classic integer-order Küpfmüller models, verified using the PID Tuner [19].

$$G_{P1D}(s) = \frac{K_p}{1+T_p s} e^{-T_d s} = \frac{1}{1+0.4934s} e^{-1.2279s} \quad (10)$$

where K_p denotes the gain of the model, T_p is the time constant and T_d is the delay of the plant.

2. Second-order dynamic plant with delay (SOPDT). The identification procedure was carried out in the same as in previous item.

$$G_{P2D}(s) = \frac{K_p}{(1+T_p s)^2} e^{-T_d s} = \frac{1}{(1+0.319s)^2} e^{-1.064s} \quad (11)$$

with the same symbols as in (10).

3. Non-integer order dynamic plant with delay (NIOPDT). Identification of the fractional order model was performed in the FOMCON toolbox for MATLAB, analogically to previous integer order models by minimization of the error cost function, using the Heaviside unit step response evaluated in the time domain with implementation of the Grünwald-Letnikov definition (3)–(4) and Trust-Region for LSA (9) optimization algorithm [20, 34]. Using formula (11) as the initial approximation of the model, after several iterations we obtained the following fractional order transfer function (FOTF) (see Fig. 4):

$$G_{PFD}(s) = \frac{K_p}{a_n s^{\nu_n} + a_{n-1} s^{\nu_{n-1}} + \ldots + a_0 s^{\nu_0}} e^{-T_d s} = \\ = \frac{1}{0.18234 s^{1.9909} + 0.65536 s^{0.98319} + 0.9992} e^{-s}. \quad (12)$$

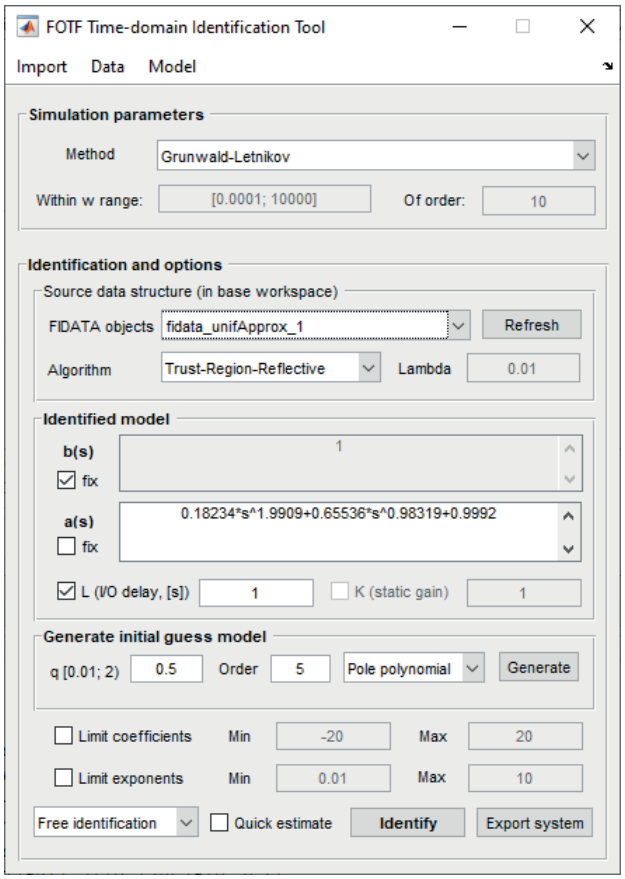

Fig. 4. FOMCON identification tool [34] used for obtaining fractional plant model (4)

It should be noted that in order to simplify the simulations of the plant models on a microcontroller, the K_p gains in (10)–(12) were set to 1. In a typical closed-loop control system, the process variable PV (e.g. temperature of a furnace) depends on the control signal of the controller actuator (the power of the heating system), namely the control variable CV, based usually on a nonlinear characteristic curve [35]. In this application, the angle assumed by the arm (the number of encoder impulses) and the rotation speed of the propeller attached to the BLDC motor are functions of the average power applied to the motor, specifically the duty cycle of the PWM signal D on the motor driver input $P_{\mathrm{AVG}} = P_{\mathrm{PEAK}} \cdot D$.

Stability of the identified models was determined following the Theorem 1. With tested order $q = 0.01$ (refer to (5)–(7) in Definition 3) the non-integer order model (12) remains stable as can be noticed in Fig. 5. Also, for integer-order models all the poles are placed on the left half of the complex plane (Fig. 6 and 7).

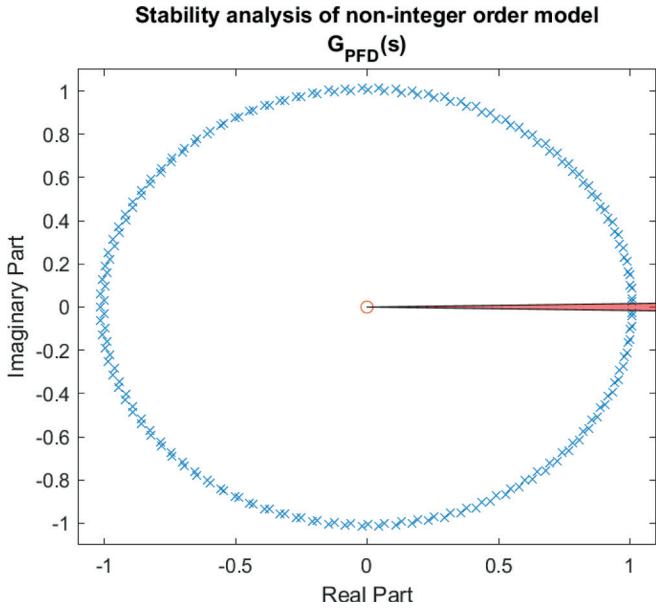

Fig. 5. Stability analysis for non-integer order model $G_{PFD}(s)$ (12)

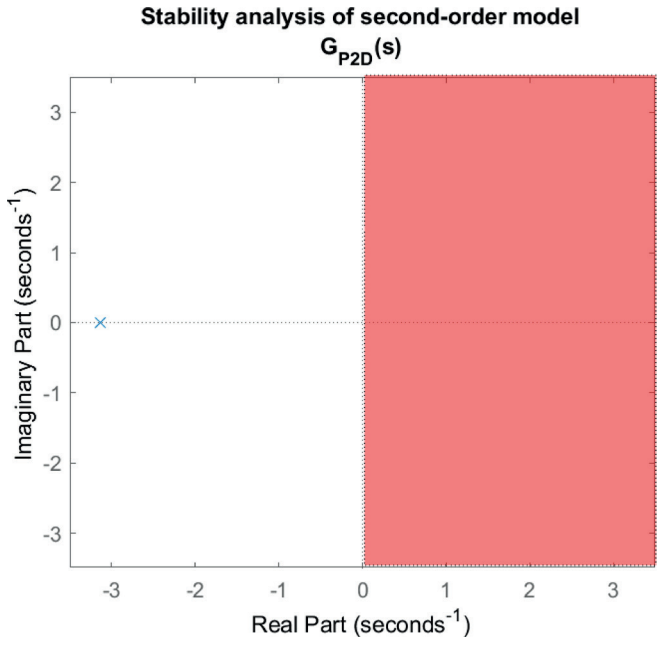

Fig. 6. Stability analysis of second-order model $G_{P2D}(s)$ (11)

The accuracy of the models was evaluated based on simulation in time $t_{sim} = 5$ s and presented as the maximum absolute percentage error (MaxAPE) and normalized root mean squared error (NRMSE) indicators and performance indices ISE, IAE, ITSE and ITAE, listed in Table 2, 3.

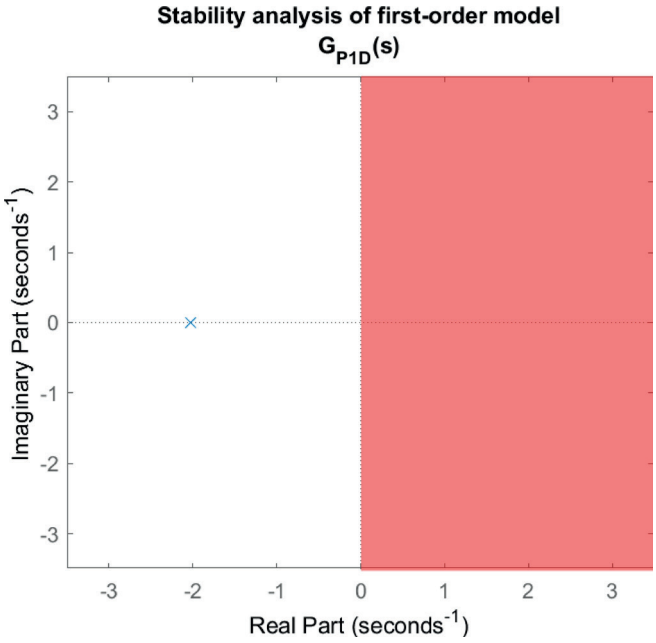

Fig. 7. Stability analysis of second-order model $G_{P1D}(s)$ (10)

Table 2

ISE $\left(\int_0^t e^2(t)\,\mathrm{d}t\right)$, IAE $\left(\int_0^t |e(t)|\,\mathrm{d}t\right)$ and ITSE $\left(\int_0^t te^2(t)\,\mathrm{d}t\right)$ matching the models with acquired data series

Type	ISE	IAE	ITSE
FOPDT	6.9119E-03	1.2005E-01	1.2433E-02
SOPDT	3.0031E-03	7.8585E-02	5.6329E-03
NIOPDT	9.6876E-04	4.6558E-02	1.5373E-03

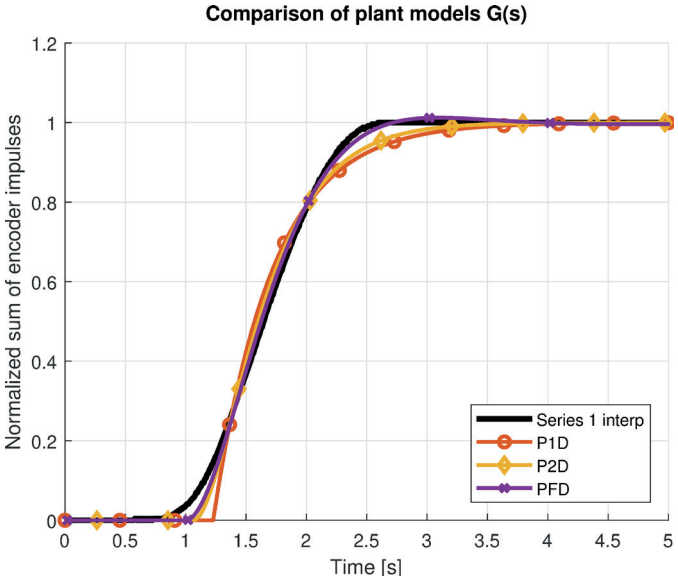

Fig. 8. Comparison of step responses of the proposed models

Table 3

ITAE $\left(\int_0^t t\,|e(t)|\,\mathrm{d}t\right)$, NRMSE $\left(1-\frac{\sqrt{\sum_{t=1}^{T} e(t)^2}}{T\,(y_{\max}-y_{\min})}\right)$ and MaxAPE $\left(\max\frac{|y_{m,i}-y_{p,i}|}{y_{m,i}}\right)$ matching the models with acquired data series

Type	IITAE	NRMSE	MaxAPE
FOPDT	2.4559E-01	91.15%	1.1725E+03
SOPDT	1.5759E-01	94.17%	1.9555E+04
NIOPDT	9.7150E-02	96.68%	6.4508E+03

5. Conclusions

This paper has presented a comparison that provides a basis and supports possibilities of novel approach to modelling using fractional-order differential equations, which was applied in the case of an electrical driver with a brushless micro-motor. Based on real system responses, well-known classical integer models (FOPDT, SOPDT) as well as fractional-order models were designed. Identification of the plant was performed using classic integer-order Küpfmüller models and verified with MATLAB Toolboxes. Synthesis of the final fractional-order form of the model was achieved in the FOMCON toolbox using the Grünwald-Letnikov algorithm with minimization of the chosen error cost function [19, 34]. The results (incl. NRMSE 96.68%) show that the fractional-order model has the best fit with the original brushless DC motor response. However, the application of fractional-order operators has some performance vulnerabilities, due to the huge number of calculation operations required for each iteration of the algorithm. This means that when dealing with fast changing systems or processes, there is the risk of insufficient microcontroller computing power. Optimization of the digital implementation of fractional-order models on a microcontroller is further described in [36].

Acknowledgements. This research was conducted under grant no. DEC-2016/23/B/ST7/03686.

References

[1] A.A. Kilbas, H. Srivastava, and J.J. Trujillo, *Theory and Applications of Fractional Differential Equations*, vol. 204, New York, NY, USA: Elsevier Science Inc, 2006.

[2] I. Podlubny, *Fractional Differential Equations. An Introduction to Fractional Derivatives, Fractional Differential Equations, to Methods of their Solution and some of their Applications*, San Diego, California: Academic Press, 1999.

[3] K.S. Miller and B. Ross, *An Introduction to the Fractional Calculus and Fractional Differential Equations*, New York: John Wiley & Sons, 1993.

[4] Y. Chen, I. Petráš, and D. Xue, "Fractional order control – A tutorial", in *Proceedings of the American Control Conference*, (St. Louis, MO, USA), 2009.

[5] A.M. Lopes and J.A. Tenreiro MacHado, "Fractional-order model of a non-linear inductor", *Bull. Pol. Ac.: Tech.* 67 (1), 61–67 (2019).

[6] P.A. Laski, "Fractional-order feedback control of a pneumatic servo-drive", *Bull. Pol. Ac.: Tech.* 67 (1), 53–59 (2019).

[7] A. Gligor and T. M. Dulău, "Fractional Order Controllers Versus Integer Order Controllers", in *Procedia Eng.* 181, 538–545 (2017).

[8] L. Majka, "Using Fractional Calculus in an Attempt at Modeling a High Frequency AC Exciter", in *Lecture Notes in Electrical Engineering*, vol. 559, pp. 55–71, Springer Verlag, 2020.

[9] G.L. Grandi and J.O. Trierweiler, "Tuning of fractional order PID controllers based on the frequency response approximation method", in *IFAC PapersOnLine*, pp. 982–987, Elsevier Ltd, 2019.

[10] F. Merrikh-Bayat, N. Mirebrahimi, and M.R. Khalili, "Discrete-time fractional-order PID controller: Definition, tuning, digital realization and some applications", *Int. J. Control Autom. Syst.* 13, 81–90, 2015.

[11] O. Aydogdu and M. Korkmaz, "Optimal Design of a Variable Coefficient Fractional Order PID Controller by using Heuristic Optimization Algorithms", *Int. J. Adv. Comp. Sci. Appl.* 10 (3), 314–321 (2019).

[12] I. Petráš and B.M. Vinagre, "Practical application of digital fractional-order controller to temperature control", *Proc. Acta Montanistica Slovaca* 7 (2), 131–137 (2002).

[13] P. Ostalczyk and P. Duch, "Closed – Loop system synthesis with the variable-, fractional – Order PID controller", in *2012 17th International Conference on Methods and Models in Automation and Robotics, MMAR 2012*, 2012.

[14] J. Baranowski, W. Bauer, M. Zagórowska, and P. Piątek, "On Digital Realizations of Non-integer Order Filters", *Circuits Syst. Signal Process.* 35 (6), 2083–2107 (2016).

[15] I. Petráš, S. Grega, and L. Dorčák, "Digital Fractional Order Controllers Realized by PIC Microprocessor: Experimental Results", tech. rep., Department of Informatics and Process Control, 5 2003.

[16] P. Ostalczyk, D.W. Brzeziński, P. Duch, M. Łaski, and D. Sankowski, "The variable, fractional-order discrete-time PD controller in the IISv1.3 robot arm control", *Cent. Eur. J. Phys.* 11 (6), 750–759 (2013).

[17] A. Rhouma and H. Sami, "A Microcontroller Implementation of Fractional Order Controller", *Int. J. Contr. Syst. Robot.* 2, 122–127 (2017).

[18] A. Tepljakov, E. Petlenkov, and J. Belikov, "Embedded system implementation of digital fractional filter approximations for control applications", in *Proceedings of the 21st International Conference on Mixed Design of Integrated Circuits and Systems, MIXDES 2014*, 2014.

[19] MathWorks, "System Identification for PID Control – MATLAB\Simulink".

[20] A. Tepljakov, E. Petlenkov, and J. Belikov, "FOMCON: a MATLAB Toolbox for Fractional-order System Identification and Control", *Int. J. Microelectron. Comp. Sci.* 2 (2), 51–62 (2011).

[21] A. Tepljakov, E. Petlenkov, and J. Belikov, "Closed-loop identification of fractional-order models using FOMCON toolbox for MATLAB", in *Proceedings of the Biennial Baltic Electronics Conference, BEC*, 2014.

[22] B.B. Alagoz, A. Tepljakov, A. Ates, E. Petlenkov, and C. Yeroglu, "Time-domain identification of One Noninteger Order Plus Time Delay models from step response measurements", *International Journal of Modeling, Simulation, and Scientific Computing* 10 (1), 19410112 (2019).

[23] K. Diethelm, *The Analysis of Fractional Differential Equations*, Springer-Verlag Berlin Heidelberg, 2010.

[24] L. Dorčák, "Numerical Models for the Simulation of the Fractional-Order Control Systems", Slovak Academy of Sciences, Institute of Experimental Physics, 1994.

[25] A. Oustaloup, *La dérivation non entière: théorie, synthèse et applications*, Paris: Hermes, 1995.

[26] P. Ostalczyk, P. Duch, and D. Sankowski, "Fractional-Order Backward-Difference Grünwald-Letnikov and Horner Simplified Forms Evaluation Accuracy Analysis", *Automatyka* 15 (3), 443–453 (2011).

[27] D.W. Brzeziński and P. Ostalczyk, "The Grünwald-Letnikov formula and its equivalent Horner's form accuracy comparison and evaluation for application to fractional order PID controllers", in *2012 17th International Conference on Methods and Models in Automation and Robotics, MMAR 2012*, 2012.

[28] D.W. Brzeziński and P. Ostalczyk, "About accuracy increase of fractional order derivative and integral computations by applying the Grünwald-Letnikov formula", *Commun. Nonlinear Sci. Numer. Simul.* 40, 151–162 (2016).

[29] P. Ostalczyk, "Remarks on five equivalent forms of the fractional-order backward-difference", *Bull. Pol. Ac.: Tech.* 62 (2), 271–278 (2014).

[30] STMicroelectronics, "STM32F745xx STM32F746xx ARM-based Cortex-M7 32b MCU+FPU, 462DMIPS up to 1MB Flash/320+16+4KB RAM, USB OTG HS/FS, ethernet, 18TIMs, 3ADCs, 25 com itf, cam & LCD Datasheet – production data", 2016, [Online]. Available: https://www.st.com/resource/en/datasheet/stm32f746zg.pdf [Accessed: 17-Apr-2020].

[31] Omron, "E6B2-CWZ6C 1000P/R 2M | OMRON Industrial Automation", 2019, [Online]. Available: http://www.ia.omron.com/product/ item/2450/ [Accessed: 17-Apr-2020].

[32] ABC-RC, "A2212 – 1000KV BLDC Brushless Motor 2-3S – 135W", 2020, [Online]. Available: https://abc-rc.pl/product-pol-6764-Silnik-ABC-Power-A2212-1000KV-2-3S-135W-ciag-820g.html [Accessed: 17-Apr-2020].

[33] S. Kamalasadan and A. Hande, "A PID Controller for Real-Time DC Motor Speed Control using the C505C Microcontroller", *17 th International Conference of Computer Applications in Industry and Engineering* 850, 34–39 (2004).

[34] A. Tepljakov, E. Petlenkov, and J. Belikov, "FOMCON: Fractional-Order Modeling and Control Toolbox for MATLAB", in *MIXDES 2011, 18th International Conference "Mixed Design of Integrated Circuits and Systems"*, Gliwice, Poland, 2011, pp. 684–689.

[35] W.Y. Svrcek, D.P. Mahoney, and B.R. Young, *A Real-Time Approach to Process Control*, John Wiley & Sons, Ltd, 2nd ed., 2007.

[36] M. Matusiak, M. Bąkała, and R. Wojciechowski, "Optimal Digital Implementation of Fractional-Order Models in a Microcontroller", *Entropy* 22, 366 (2020).